Electron-phonon quantum kinetics in the strong-coupling regime

D. Steinbach, G. Kocherscheidt, M. U. Wehner, H. Kalt, and M. Wegener
Institut für Angewandte Physik, Universität Karlsruhe (TH), Kaiserstraße 12, D-76128 Karlsruhe, Germany

K. Ohkawa and D. Hommel
Institut für Festkörperphysik, Universität Bremen, Kufsteinerstraße NW1, D-28359 Bremen, Germany

V. M. Axt
Institut für Theoretische Physik II, Universität Münster, Wilhelm-Klemm Straße 10, D-48149 Münster, Germany

(Received 11 January 1999)

The quantum kinetics of optically excited crystal electrons coupled to a bath of dispersionless phonons is studied in the regime of strong electron-phonon coupling. Four wave-mixing experiments on a thin film of bulk ZnSe using 13 fs blue pulses give evidence for corresponding effects that are distinctly different from those found for GaAs which has proven to be a model system for the weak-coupling regime. The experimental results on ZnSe are compared with solutions of a simple model Hamiltonian of electron-phonon interaction suitable for both GaAs and ZnSe. Exact analytic solutions of this model for arbitrary electron-phonon coupling strengths are compared with numerical solutions of the same model following the usual approach in terms of an infinite hierarchy of correlation functions. Virtues and limitations of the simple model Hamiltonian with respect to the experiment are discussed. [S0163-1829(99)10441-7]

I. INTRODUCTION

Relaxation and scattering processes in semiconductors, such as, e.g., electron-phonon scattering, are often thought of as inherently dissipative processes which happen at a certain instant in time and at a certain rate. Recent progress in quantum kinetic theories as well as progress in experimental techniques has shown that this is not true on a time scale of several tens of femtoseconds.[1–5] In this time regime—the quantum kinetics regime—the finite duration of the scattering process leads to several qualitatively new features: the dynamics becomes non-Markovian, energy conservation for the individual scattering process is not given due to time-energy uncertainty, and the scattering process has not become irreversible yet. Clearly, such situation can no longer be described by effective scattering times as in the Boltzmann kinetics or as derived from Fermi's golden rule. Early experiments on electron-phonon quantum kinetics were published a few years ago and were performed on bulk GaAs.[6] In these four-wave mixing (FWM) experiments with optical pulses of about 10 fs in duration, the electron-phonon quantum kinetics showed up as an oscillation which is superimposed on the exponential decay of the coherent FWM signal. Later, pump/probe experiments on bulk GaAs have also shown quantum kinetic effects.[7] Here the time-energy uncertainty leads to initially broad phonon satellites in the differential transmission spectrum which sharpen up for longer times, eventually approaching the Boltzmann limit. In FWM experiments on GaAs quantum well structures,[8] the oscillation is sine shaped—in contrast to bulk GaAs where it is close to a cosine oscillation. In Ref. 8 we have also presented an extensive discussion concerning quantum kinetics effects on one hand and coherent phonons[9] on the other hand and as to how these two distinctly different pieces of physics can be distinguished experimentally. Finally, applying the general idea of coherent control[10–16] to the electron-phonon quantum kinetics, we have shown that the uncompleted electron-phonon scattering event can indeed be reversed or enhanced[17] for times as long as 60 fs after initial optical excitation.

Most of the underlying physics is quite general and GaAs has merely served as a well-defined model system. A crucial parameter for the electron-LO-phonon coupling, however, is the electron-phonon coupling constant which can be rewritten into the dimensionless Fröhlich constant α. The importance of this parameter becomes clear when we consider scattering events of electrons with simultaneous emission of n phonons, the relative strength of which scales as α^n. In GaAs ($\alpha=0.06$) one is within the weak-coupling regime and scattering processes of an electron with one phonon are sufficient to understand the dynamics. Equivalently, the second-order Born approximation is valid. In ZnSe, the Fröhlich constant is almost one order of magnitude larger ($\alpha=0.43$) than in GaAs and we expect additional new features with respect to GaAs.

So far, to our knowledge, no other experiments have been reported on bulk ZnSe using pulses of 10 fs in duration. A large number of experiments using 100-fs pulses, however, have addressed aspects of the dynamics in ZnSe different than quantum kinetics. These papers highlight the yet increased importance of excitonic effects in ZnSe compared to GaAs due to its large excitonic binding energy. Coherent transient phenomena of excitons have been investigated by time-integrated and time-resolved FWM, revealing a free induction decay of excitons and a quantum beat behavior of heavy-hole and light-hole excitons.[18,19] High-order contributions to the FWM signal dominated by excitonic resonances have been observed implying nonlinear effects beyond the pertubative regime.[20] In this work, also decay rates associated to exciton-LO-phonon scattering have been determined showing that this scattering mechanism is much stronger in ZnSe than in GaAs—as expected from our above discussion. This behavior has also been observed in two-dimensional ZnSe structures.[21,22] In polarization-dependent FWM experi-

ments, a contribution of biexcitons, mainly at negative time delays, has been identified. This contribution has been clearly separated from the excitonic resonance.[23,24] Finally, Ref. 25 has studied the relaxation of excitons in their center of mass parabola in ZnSe quantum wells. The strong electron-LO-phonon coupling of ZnSe together with its large exciton binding energy leads to a relaxation dynamics which is distinctly different compared to GaAs.

This article is organized as follows. In Sec. II we describe the experimental setup in some detail—a reader only interested in semiconductor physics may skip this section. In Sec. III we present our recent results on bulk ZnSe using optical pulses of about 10 fs in duration. In particular, we present experimental data on (i) the density dependence, (ii) coherent control, and (iii) conventional three-pulse experiments. We then discuss the experimental evidence in terms of a simple phenomenological model Hamiltonian in Sec. IV. After discussing its analytical solutions which are obtained by means of generating functions in the short excitation pulse limit for arbitrary phonon coupling strengths, we compare these results with numerical solutions using the usual density matrix formalism. Both types of results are compared with the experiment which shows the virtues and limitations of this simple model. We finally conclude in Sec. V.

II. EXPERIMENTAL SETUP

(a) *Laser source*. Experiments in the quantum kinetic regime performed on bulk ZnSe with resonant optical excitation require a femtosecond laser source in the blue spectral range according to the band gap of ZnSe, which is around 2.82 eV at 77 K. Since direct generation of ultrashort pulses in this spectral range is currently not possible, many approaches have used indirect methods.[26–28] We use a laser system slightly modified with respect to Ref. 29 to generate sech^2-shaped optical pulses of 13.0 fs in duration [full width at half maximum (FWHM)] at 438-nm center wavelength by extracavity frequency doubling of a 10.8-fs Ti:sapphire oscillator operating at 880-nm center wavelength using a 100-μm thick beta-bariumborate (BBO) crystal. The dispersion of the FWM setup is precompensated in a sequence of prisms and chirped mirrors.

(b) *Details of the laser source*. The fundamental pulses in the near infrared are generated by a home-built Ti:sapphire laser with a design closely similar to Ref. 30. The gain medium is a 4.75-mm-long Ti:sapphire rod and two fused silica prisms are used to control the dispersion inside the resonator (separation 52 cm). The duration-bandwidth product of the sech^2-shaped 10.8 fs pulses (FWHM) is 0.320, which is close to the theoretical limit (0.315). By using an adequate mirror set (minimal dispersion at 870-nm wavelength), the wavelength can be tuned to 880 nm. The dispersion of the output coupler and the following components introduced into the beam has been precompensated by a first four-prism (fused silica) sequence. Great care has been taken that the optical path of the near-infrared pulses is equivalent for both the autocorrelation and the frequency doubling setup. The average power of the fundamental pulses in front of the BBO second-harmonic generation (SHG) crystal is 440 mW. The pulses are focused onto a 100-μm-thick BBO crystal by a $f=75$ mm focal length lens with the BBO cut at $\Theta=24°$ for type-I phase matching and antireflection coated for 800-nm wavelength. They are collected by a 30-mm focal length lens in order to effectively reduce the beam diameter to 40% of the incoming one. This subsequently limits the amount of undesired glass inserted into the beam by the following four-prism sequence (fused silica) for dispersion compensation of the autocorrelator and the FWM experiment. The tip to tip prism separation is 180 mm. A simple four-prism sequence alone, however, is not able to eliminate *both* second- and third-order dispersion in the blue spectral range. Forty-two reflections, realized by a sequence of four dielectric dispersive mirrors[31] (chirped mirrors) is introduced as an additional element of dispersion compensation. The dispersion of yet higher-order dispersion can be kept moderate due to the small amount of glass introduced by the prisms. The resulting average power of the second harmonic pulses after the dispersion (pre-) compensation is 24 mW. All glass elements of the autocorrelator for the blue pulses and the FWM experiment are made of fused silica. The pulses are focused onto the autocorrelator SHG crystal by a 100-mm focal length lens, the beam separation before the lens is 3 mm. The SHG crystal is again a free-standing BBO with a thickness of 20 μm cut at $\Theta=79°$ for type-I phase matching. This altogether results in the generation and detection of 13.0-fs sech^2-shaped pulses centered at 438-nm wavelength, which have a bandwidth of 156 meV corresponding to a duration-bandwidth product of 0.47. A certain fraction of the value of 13.0 fs is limited by the extreme requirements to the autocorrelator SHG crystal.[29] The inevitable finite thickness of the free-standing autocorrelator doubling crystal prevents frequency components on the wings of the very broad spectrum to fulfill the usual phase-matching condition.[29] For this reason, the actual duration of the blue pulses could be shorter than the measured value of 13.0 fs. In fact, the Fourier-transform of the well-behaved laser spectrum supports a 8.4-fs pulse (following Ref. 32). The spectrum of the blue pulses is roughly resonant with the band edge of ZnSe as can be seen in the inset of Fig. 2.

(c) *Four-Wave Mixing and Coherent Control Setup*. The blue laser beam is split up in a modified Michelson interferometer in two or three identical pulses of equal linear polarization and equal intensity. Great care has been taken to assure that all pulses experience the same number of reflections and pass the same number of beam splitters inside the interferometer. We use highly reflective dielectric mirrors and beam splitters which are superior to metallic ones in terms of losses—a point which is important given the low average power of the laser source. The group velocity dispersion of the dielectric mirrors is sufficiently small only for the polarization component perpendicular to the plane of incidence. Their dispersion can easily be precompensated. The time delay between the pulses is varied by piezoelectric actuators. The pulses are focused onto the sample by a fused silica lens ($f=100$ mm). The FWM signal is recorded as a function of the time delay between the pulses either via a photomultiplier tube or spectrally resolved by a 0.25-m spectrometer connected to a nitrogen-cooled charge-coupled device (CCD) camera. The polarization of one pulse can be rotated by 90 degrees with respect to the other ones by a half wave plate in front of the sample. In FWM experiments using coherent control over the system, phase-locked pulses are re-

quired. The semiconductor is excited by a first pulse while a second pulse with a suitable relative phase to the first one allows to modify the scattering event. Together with the third pulse the FWM signal is generated. The phase-locked pulses are derived from an apparatus similar to the one described in Ref. 33, which meets two important demands for a time-resolved interferometric experiment: (i) active stabilization of the relative phase between the phase-locked pulses and (ii) continuous, calibrated scanning of their time delay over a wide range. The setup is quite simple. One blue laser line of an argon-ion laser (457.9 nm) is alligned parallel to the blue pulses in the two arms of the interferometer. In one arm the polarization of the 457.9-nm line is rotated to polarization parallel to the plane of incidence by introducing a $\lambda/2$ retardation plate. Behind the interferometer the parallel and vertically polarized beams are transformed into left and right circularly polarized beams, respectively, by a $\lambda/4$ retardation plate. These oppositely circularly polarized beams, ideally of equal intensity, lead to linearly polarized light. The plane of polarization depends only on their relative phase. After passing an analyzer, the axis of which includes a variable angle with the plane of the setup, the resulting intensity is detected with a photodiode, which is the input to a conventional proportional-integral-differential amplifier controlling the length of one arm of the interferometer by driving a piezoelectric actuator and in this way keeping the signal on the photodiode constant. Thus any phase drift of the phase-locked pulses induces a change of the voltage applied to the piezoelectric actuator which in turn compensates the phase drift. The phase, on the other hand, can be continuously changed and accumulated by rotating the angle of the analyzer. In this way it is possible to scan the time delay of the phase-locked pulses and the analyzer serves as an optical screw that changes the time delay between the phase-locked pulses.

(d) *Sample*. The sample is a high quality ZnSe film grown on a GaAs substrate and a 300-nm buffer layer by molecular beam epitaxy with a thickness of the coherently strained bulk ZnSe layer of 100 nm resulting in a small optical density of 0.2 for continuum states at a lattice temperature of 77 K. This minimizes propagation effects on the time scale discussed here.[34] The sample is glued to a sapphire substrate, the GaAs substrate is removed by grinding and etching and this side of the sample is antireflection coated by evaporating a single quarter wave layer of HfO_2. The ZnSe film is biaxially compressed due to the lattice mismatch of 0.24% at 77 K of ZnSe grown on GaAs which results in a splitting of the heavy-hole (hh) and the light-hole (lh) exciton of 10.6 meV (well separated from the LO-phonon energy of $\hbar\omega_{\mathrm{LO}} = 31.8\,\mathrm{meV}$) corresponding to a beat period of 390 fs. The thickness of the ZnSe film is well below the critical thickness for nucleation of misfit dislocations.[35] The sample is kept in a liquid-nitrogen cryostat at 77 K. The linear absorption spectrum at 77 K, measured by a white light continuum, is depicted in the inset of Fig. 2. The electron-hole densities quoted in the following are determined via the measured total incident flux and the spot radius of 13 μm, measured with a knife edge technique at the sample location. For the effective absorption coefficient we have used 75% of the measured unsaturated continuum value of $4.6\times10^4\,\mathrm{cm}^{-1}$ since about 75% of the laser spectrum is above the excitonic resonances.

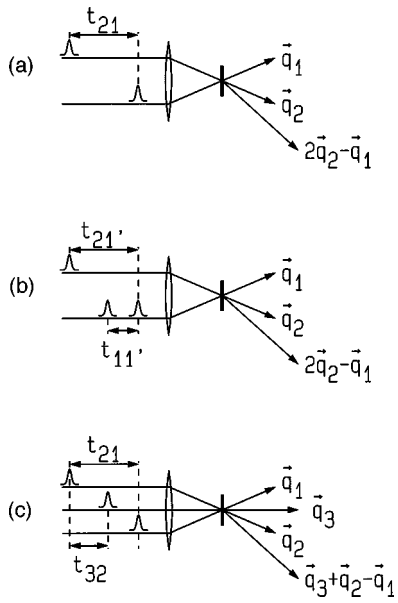

FIG. 1. Schematic of the three different types of four-wave mixing (FWM) experiments discussed in this article. (a) Two-pulse experiment, (b) coherent control, and (c) three-pulse experiment configuration.

III. FOUR-WAVE MIXING EXPERIMENTS

The geometry of the three different FWM experiments is shown in Fig. 1. For the two-pulse experiment [Fig. 1(a)], two pulses with wave vectors $\vec{q}_1$ and $\vec{q}_2$, respectively, arrive at the sample at times t_1 and t_2. The diffracted signal in direction $2\vec{q}_2-\vec{q}_1$ is recorded as a function of the time delay, defined according to $t_{21}:=t_2-t_1$. For the coherent control experiment [Fig. 1(b)] two phase-locked pulses 1 and $1'$ are separated by the time delay $t_{11'}:=t_1-t_{1'}$, which can be kept constant within ±40 attoseconds corresponding to a motion of one of the mirrors in the interferometer of ±6 nm, and propagate collinearly in the direction $\vec{q}_1=\vec{q}_{1'}$. Interaction with the third pulse (2) propagating along wave vector $\vec{q}_2$ with the time delay $t_{21'}:=t_2-t_{1'}$ leads to two nonequivalent diffracted FWM signals with wave vectors $2\vec{q}_2-\vec{q}_1$ and $2\vec{q}_1-\vec{q}_2$, respectively. Here we focus the experiments on the emission in the direction $2\vec{q}_2-\vec{q}_1$ for which, in the $\chi^{(3)}$ regime, the phase-locked pulses enter linearly. The three-pulse geometry is finally shown in Fig. 1(c). Note that the signal in direction $\vec{q}_3+\vec{q}_2-\vec{q}_1$ is symmetric in the time delays t_{21} and t_{31}. The usual two-pulse experiment is recovered for the special case $t_{32}=0$, $\Leftrightarrow t_{31}=t_{21}$ (for excitation within the $\chi^{(3)}$ regime).

A. Two-pulse Experiments

One example of the time-integrated two-pulse FWM signal for parallel ($\parallel$) and orthogonal ($\perp$) linear polarization of the two incident pulses is shown in Fig. 2. Oscillations with the LO-phonon period $T_{\mathrm{LO}}=131\,\mathrm{fs}$ of ZnSe ($\Leftrightarrow\hbar\omega_{\mathrm{LO}} = \hbar 2\pi/T_{\mathrm{LO}}=31.8\,\mathrm{meV}$) are superimposed on the decay of the coherent FWM signal. The LO-phonon oscillation period

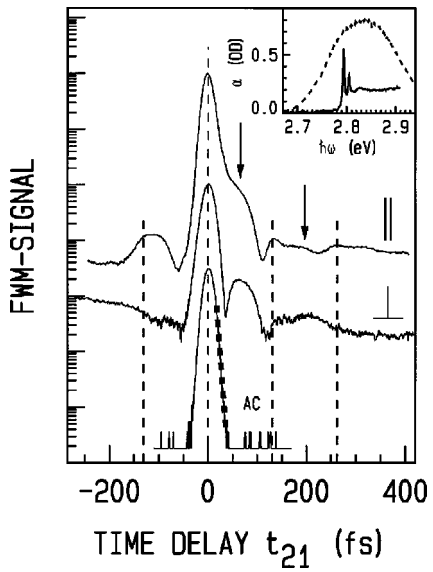

FIG. 2. Two-pulse FWM signal versus time delay, bulk ZnSe, $T=77$ K, $n_{eh}=2.6\times10^{17}\,\mathrm{cm}^{-3}$. Results for parallel (∥) and perpendicular (⊥) linear polarization of the two incident pulses are shown on the same scale. The dashed lines at integer multiples of the LO-phonon oscillation period (131 fs) are guides for the eye. The arrows indicate oscillatory structures which are associated with twice the LO-phonon oscillation frequency. The curve labeled AC is the autocorrelation of the laser pulses showing exponential wings with 7.1 fs time constant. The inset shows the linear absorption coefficient α in units of optical densities, OD ($e^{-\alpha L}=10^{-\mathrm{OD}}$), as well as the laser spectrum.

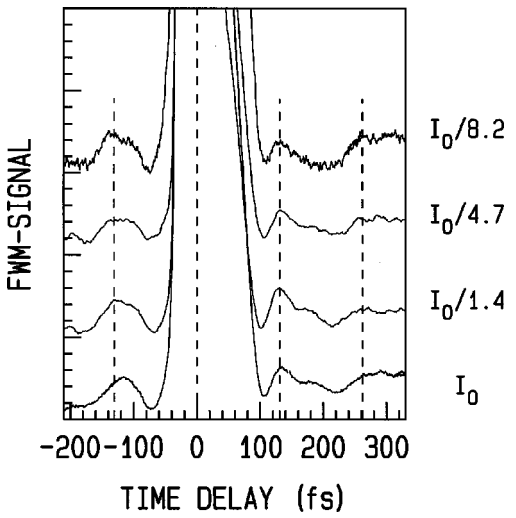

FIG. 3. Two-pulse FWM signal as Fig. 2 (∥ configuration) on a linear scale. The excitation density is parameter. I_0 corresponds to a density of $n_{eh}=5.1\times10^{17}\,\mathrm{cm}^{-3}$. All curves are normalized to their peak value and the large peak around $t_{21'}=0$ is truncated.

is indicated by the dashed lines at integer multiples of the phonon oscillation period. The excitation density of $n_{eh}=2.6\times10^{17}\,\mathrm{cm}^{-3}$ is within the low excitation density—a point which will be addressed in more detail below. Even though the absolute carrier density seems quite large at first, one must remember that the relevant quantity is $n_{eh}r_B^3$ with the excitonic Bohr radius r_B. Thus a density of $n_{eh}=5.1\times10^{17}\,\mathrm{cm}^{-3}$ in ZnSe ($r_B=3.9$ nm) is comparable to a density of $n_{eh}=2\times10^{16}\,\mathrm{cm}^{-3}$ for GaAs ($r_B=12.5$ nm). Besides structures with the phonon period $T_{\mathrm{LO}}=131$ fs, also additional weaker structures at twice the phonon frequency (corresponding to half the phonon period of $T_{\mathrm{LO}}/2=65$ fs) are observed (see arrows in Fig. 2, ∥). It is important to note that each of these structures is distinctly different from both the hh-lh splitting, corresponding to an oscillation period of 390 fs, and the inverse exciton Rydberg energy of 19 meV, corresponding to a beat period of 218 fs. It can be ruled out also that the inverse of the sum of LO phonon and exciton Rydberg energy, $31.8\,\mathrm{meV}+19\,\mathrm{meV}=50.8\,\mathrm{meV}$, corresponding to an oscillation period of 81.5 fs, is consistent with any of the observed structures.

We have also varied the orientation of the two equally polarized pulses with respect to the ZnSe crystal axes by introducing a free standing, zero-order half wave plate in front of the sample. No dependence of the line shape of the FWM signal is found.

The signal with the orthogonal configuration (⊥) is two orders of magnitude weaker than for the ∥ case (Fig. 2) revealing detailed information on the spin dependence of the physics involved. A process in which a spin-up (-down) electron exclusively couples to a spin-up (-down) electron, such as, e.g., Pauli blocking, would show no polarization dependence, so the signals in both polarization configurations should be equal. However, a coupling to the sum of spin-up and spin-down contributions[36] would indeed lead to a complete cancellation of the signal in the orthogonal case. The polarization dependence seen in Fig. 2 thus also excludes hh-lh beating of continuum states[37] for the results in the parallel configuration. This mechanism, which is based on Pauli blocking, would give different signals for the two polarization configurations ∥ and ⊥, but both signals would have comparable strengths which is inconsistent with our data (Fig. 2).

In order to exclude an interpretation of the oscillations in terms of Rabi or plasmon oscillations we have also investigated the dependence of the FWM signal on the excitation density (Fig. 3) which is varied by means of neutral density filters. Reducing the excitation density up to a factor of about 10 leaves the shape of the FWM signal essentially unaffected. The periods of the oscillatory structures and their strength remain unchanged, for even lower densities the worse signal/noise ratio inhibits a detailed analysis. The density independence also rules out any interpretation of the oscillations in terms of coherent phonons. It has been shown previously [8] that coherent phonons,[9] i.e., a coherent nonequilibrium oscillation of the lattice displacement, would not show up in a FWM experiment in the low excitation density limit, but would appear at elevated excitation densities only. Such density dependence, however, is clearly not observed here (Fig. 3) which rules out that coherent phonons play a dominant role under these conditions.

The spectrally resolved FWM signal for parallel polarization is shown in Fig. 4. It exhibits a purely excitonic response with two narrow peaks at the hh and the lh resonance but no indications of satellites around one or two LO-phonon energies to the low- or to the high-energy side. The same is observed for the orthogonal configuration (not shown). This unexpected behavior is consistent with the experiments in the weak-coupling regime previously performed on bulk

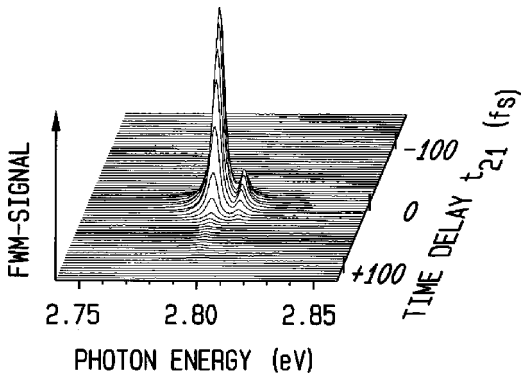

FIG. 4. Spectrally resolved two-pulse FWM experiment under the same conditions as Fig. 2, ∥ configuration, plotted on a linear scale. Two peaks, one at the heavy-hole and another at the light-hole exciton, are observed, but no phonon satellites occur.

GaAs.[6] It should also be noticed that the FWM spectra do not show indications of propagation effects.[34]

We assign the structures with the simple LO-phonon oscillation period and twice the LO-phonon frequency (Fig. 2) to scattering processes with simultaneous emission of one and two phonons, respectively. Intuitively, this means that coherence of an electron is preserved for some time even if it emits one or two phonons in a single step. This interpretation will be confirmed by the model calculations presented below. First, however, we want to present additional data using the concept of coherent control.

B. Coherent control experiments

In a general sense, coherent control of a quantum-mechanical system means that we are able to prepare the system in any desired initial state wave function Ψ. Basic quantum mechanics tells us that this wave function can be represented in a complete orthonormal basis of eigenfunctions ϕ_n, i.e., in the form $\Psi=\Sigma_n a_n e^{i\varphi_n}\phi_n$. Coherent control is thus equivalent to the ability to control the real amplitudes a_n and the phases φ_n deliberately. While such complete coherent control is indeed possible in state of the art experiments on atomic systems, most experiments on semiconductors have used a much simpler form of coherent control which consists of excitation with a pair of phase-locked pulses. Recently, it has been shown that such coherent control experiments allow to suppress or amplify the one-phonon oscillation[17] and an analogous behavior is expected for the n phonon processes as well. The corresponding physics will be discussed in Sec. IV. Examples of such coherent control experiments are shown in Fig. 5 for excitation conditions comparable to Figs. 2 and 4. Here a range of values of $t_{11'}$, larger than one optical cycle (1.53 fs) around a value of $t_{11'}\approx -20$ fs, for which the optical pulses have no significant overlap, is depicted. Depending on the choice of $t_{11'}$, we either observe one-phonon oscillations but no two-phonon oscillations (e.g., $t_{11'}=-20.62$ fs) or the opposite, in a small range of $t_{11'}$ quite pronounced structures at half the phonon period and no one-phonon oscillations (e.g., around $t_{11'}=-21.24$ fs). The latter is highlighted in the inset of Fig. 5. This scenario repeats itself. The modulation becomes hardly noticeable for $t_{11'}$ beyond -160 fs. In Fig. 6, data for $t_{11'}$ in the range of -69 fs are presented, which is about half

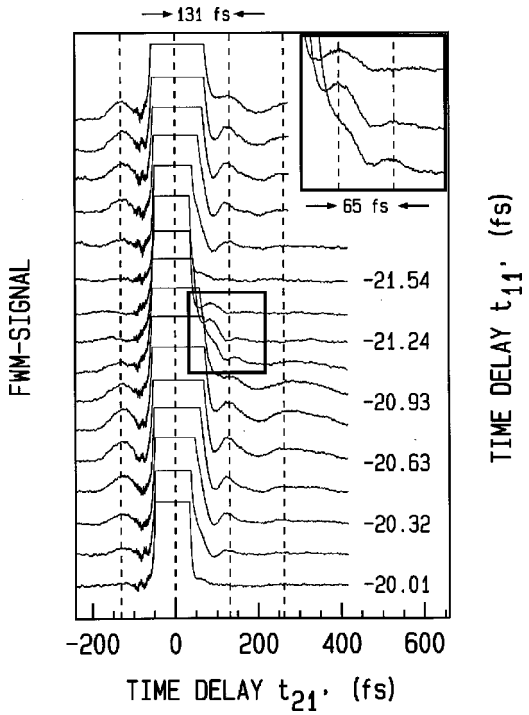

FIG. 5. Coherent control experiment under conditions similar to Fig. 1, ∥ configuration, $n_{eh}=5.1\times10^{17}\,\mathrm{cm}^{-3}$ (incoherent sum). The time delay between the phase-locked pulses, $t_{11'}$, is a parameter which is varied in steps of 0.153 fs. The curves are shown on a linear scale. For clarity, the curves are vertically displaced and the large peak around $t_{21'}=0$ is truncated. The inset highlights the promnent two-phonon oscillation.

the LO-phonon oscillation period. Here the one-phonon oscillation is hardly visible ($t_{11'}=-68.75$ fs) while the two-phonon oscillation dominates the signal. The latter is visible in a wider range of values of $t_{11'}$ (from -67.98–-68.60 fs) compared with the case $t_{11'}$ around -20 fs. For a time delay in the range of $t_{11'}\approx-130$ fs which corresponds to one LO-phonon oscillation period (not shown) the situation is inverted. Here the one-phonon oscillation is much more prominent than the two-phonon oscillation. This behavior will be explained within a simple model below. The overall behavior in the coherent control experiment in itself again rules out an interpretation of the oscillations along the lines of a hh-lh quantum beating in the band to band continuum.[37] Here one would expect a continuous change of the oscillation frequency as a function of $t_{11'}$ which is clearly not observed in our experiment.

Another interesting way to look at the coherent control signal is to plot the data as a function of the time delay $t_{11'}$ while keeping the time delay $t_{21'}$ fixed. This scanning mode is also possible with our stabilization setup. Within the low excitation density limit one simply expects an oscillation with the frequency of light which is modulated by some envelope. Beyond the third-order perturbation limit, however, contributions which propagate in the same diffracted direction as, e.g., $2\vec{q}_2+\vec{q}_1-2\vec{q}_{1'}$ and $2\vec{q}_2+\vec{q}_{1'}-2\vec{q}_1$, interfere among themselves and with the above contribution and consequently lead to components oscillating with twice and three times the laser frequency which show up as higher harmonics in the time-delay domain (but not in the real time domain). Looking at the phase factors of all third- and fifth-

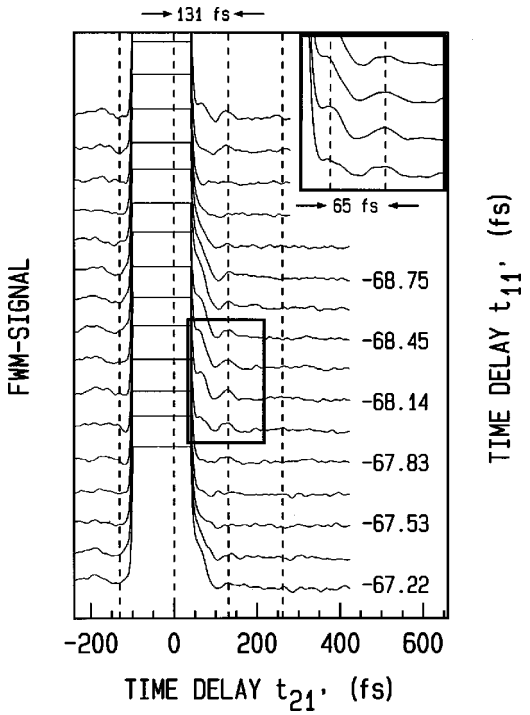

FIG. 6. Same as Fig. 5, however, for a different range of time delays $t_{11'}$. Notice that here the two-phonon oscillation dominates the dynamics.

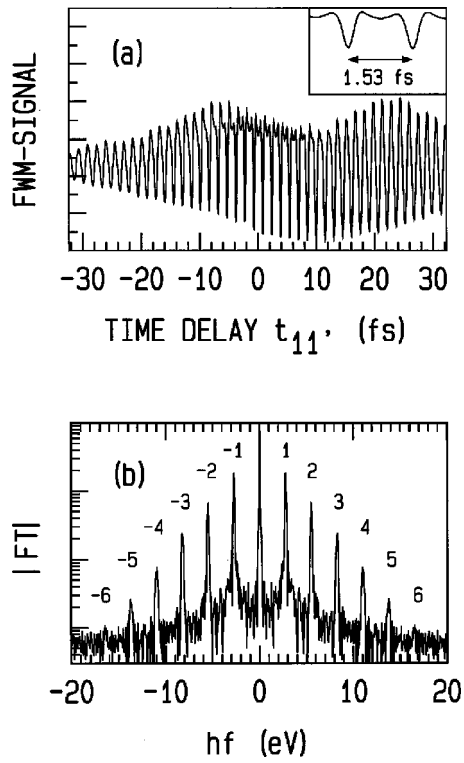

FIG. 7. (a) Coherent control experiment as Fig. 5. The FWM signal is plotted versus $t_{11'}$ for $t_{21'} \approx 0$ fs. (b) Fourier-transform of (a).

order contributions of the FWM signal propagating in the direction $2\vec{q}_2 - \vec{q}_1$ within the rotating wave approximation[38] one finds that in third order, the only occuring beat oscillation is $\omega t_{11'}$ while up to fifth order also terms like $2\omega t_{11'}$ occur. If such data are Fourier transformed with respect to $t_{11'}$, the strengths of the harmonics of the light frequency can immediately be interpreted as the strengths of the contributions from the higher-order nonlinear susceptibilities $\chi^{(n)}$.[38]

Figure 7(a) shows a typical FWM trace as a function of $t_{11'}$ for $t_{21'} \approx 0$. Besides the simple interference with the exciton transition frequency, an additional structure is observed around $t_{11'} \approx 0$. From the inset in Fig. 7(a) it can already be seen that this fine structure is related to higher frequency components which can be seen in detail when Fourier transforming the FWM signal with respect to $t_{11'}$ as shown in Fig. 7(b). Only integer harmonics of the basic laser frequency occur. The peaks labeled 1 and -1 around 2.82 eV energy are the $\chi^{(3)}$ contribution, peaks 2 and -2 correspond to the $\chi^{(5)}$ contribution and so forth. These data clearly show that the excitation densities are above the low excitation density limit ($\chi^{(3)}$). This observation has to be discussed in the context of our above statement that the shape of the FWM signal is density independent (Fig. 3) under identical conditions. These two observations together imply that even though the third-order perturbational regime is not reached in a strict sense, i.e., the signal strength does not scale according to the third power of the incident intensity, the shape of the signal is still unaffected. For the modeling discussed below, this important result means that the $\chi^{(3)}$ limit can still deliver relevant results.

C. Three-pulse experiments

In the two-pulse as well as in the coherent control experiments the FWM signal exhibits a first rapid initial decay over more than two orders of magnitude with an approximate time constant of 8 fs (see Figs. 2, 5, and 6). This time constant seems to be in conflict with the spectral half width at half maximum of the FWM spectrum of about 2 meV which corresponds to a dephasing time of 310 fs (or yet longer if the exciton line was inhomogeneously broadened). In previous works we have pointed out for the case of GaAs (Ref. 39) that the usual models for the optical nonlinearities, e.g., the optical Bloch equations or semiconductor Bloch equations with phenomenological dephasing constants, the local field model[40] or excitation induced dephasing due to exciton-exciton scattering cannot describe this aspect of the data. In fact, to our knowledge, to date no microscopic theory has explained these findings. The unusual behavior for GaAs could, however, be described phenomenologically by assuming that the dominant optical nonlinearity is due to scattering of $1s$ excitons with continuum states.[39] Intuitively, the rapid initial decay is due to an interference between the different scattering channels of $1s$ excitons with the continuum of ionization states. Thus the resulting time constant in the time delay can no longer be interpreted as a dephasing time. To further strengthen our suspicion that the mechanism is the same in ZnSe, we have also performed three-pulse experiments similar to the ones on GaAs.[39]

Figure 8 shows one example of such three-pulse FWM experiments for a total excited carrier density of $n_{eh} = 5.1 \times 10^{17}\,\mathrm{cm}^{-3}$. The signal is formed by two sharp ridges which cross and add to build the central peak for both time delays, t_{21} and t_{32}, being zero. The ridges are related to each other via symmetry, i.e., the signal does not change when the beams 2 and 3 are exchanged. The ridge around $t_{21} = 0$ fs rapidly decays on a timescale of 8 fs as a function of t_{21}. It

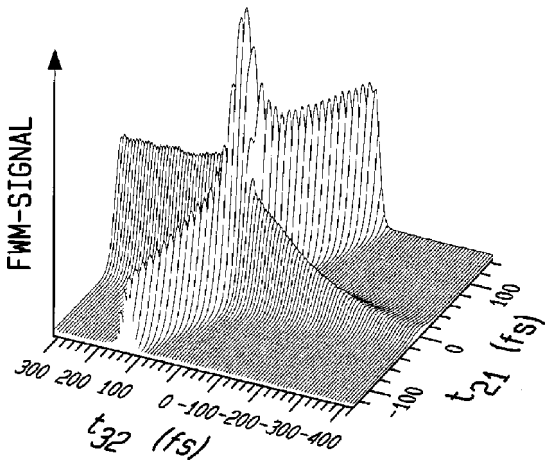

FIG. 8. Three-pulse FWM signal versus the time delays t_{21} and t_{32}. ZnSe, $T=77\,\mathrm{K}$, $n_{eh}=5.1\times10^{17}\,\mathrm{cm}^{-3}$.

is constant for positive t_{32} while it decays with a time constant of 160 fs equivalent to half the $1s$-exciton dephasing time, for negative t_{32}. This decay matches the observed spectral linewidth in the FWM-spectrum (Fig. 4) rather well. In Fig. 9 selected traces of Fig. 8 are plotted on a logarithmic scale. The trace for zero delay, i.e., $t_{21}=0$, depicts the top of the ridge with constant signal for positive delay and an exponential decay for negative delay t_{32}. Around $t_{21}=0$ fs, the FWM line shape as a function of t_{32} shows characteristic structures which have previously also been observed in similar experiments on GaAs.[39] The traces at $t_{21}=-10$ fs and $+10$ fs exhibit a minimum adjacent to the central peak, a feature which is not seen for $t_{21}=0$ fs. For larger positive values of t_{21}, additional structures can be found for positive t_{32} which can be associated to the LO-phonon oscillation period. For time delays of t_{21} near half the phonon oscillation period a distinct structure at 65 fs can be seen while for even higher values of t_{21} (110 fs) a structure at 131 fs occurs. The structures are absent for negative values of t_{21} as can, e.g., be seen for a time delay of $t_{21}=-50$ fs. The latter features have not been observed in corresponding experiments performed on bulk GaAs (Ref. 39) which suggests that they are specifically due to the strong electron-phonon coupling regime.

In the three-pulse experiment, the exciton-continuum scattering dominates while the electron-phonon scattering is more prominent in the coherent control configuration. Hence the three-pulse FWM experiments and the coherent control experiments deliver complementary information.

IV. A SIMPLE MODEL

A microscopic quantum theory for the above experiments has to account for non-Markovian electron-phonon scattering in the strong-coupling regime as well as for excitonic effects. The large exciton Rydberg energy in ZnSe as compared to GaAs, together with our above discussion on exciton-continuum scattering, means that the Hartree-Fock approximation is possibly not adequate at this point. Solutions of such a quantum theory are currently not available and it is beyond the scope of this paper to solve this challenge of many body physics.

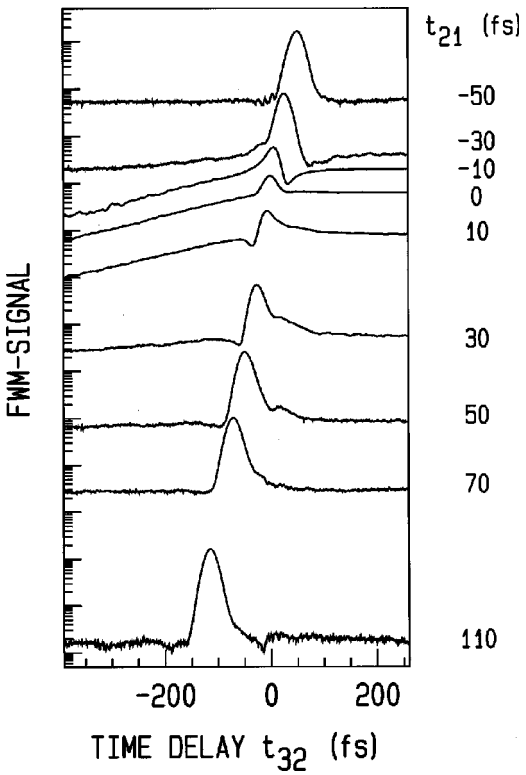

FIG. 9. Selected traces of Fig. 8, plotted on a logarithmic scale. ZnSe, $T=77\,\mathrm{K}$, $n_{eh}=5.1\times10^{17}\,\mathrm{cm}^{-3}$.

Apart from this, it is yet more important for experimentalists to develop simple pictures which allow to derive some sort of intuition for the underlying many-body physics. This has motivated us to study a very simple model Hamiltonian which consists of a fermionic two-level system with ground state $|0\rangle$ and excited state $|1\rangle$. These two states can be thought of as two states in the valence and conduction band of the semiconductor, respectively, or—not quite compatible with the Fermi statistics—as the ground state of the crystal and the $1s$-exciton state. For convenience we set the ground-state energy zero, the excited state energy is $\hbar\Omega$. The light field E at center frequency ω couples to the system via the dipole matrix element d. So far, the ingredients constitute nothing but the well-known optical Bloch equations. State $|1\rangle$, however, also couples to a single phonon mode with frequency ω_{LO} via the coupling strength g. In terms of creation and annihilation operators $c^\dagger$, c for the electrons and $a^\dagger$, a for the phonons, the Hamiltonian is given by

$$H=\hbar\Omega c_1^\dagger c_1-dE(c_1^\dagger c_0+c_0^\dagger c_1)+\hbar\omega_{\mathrm{LO}}a^\dagger a+\hbar g \times(a^\dagger c_1^\dagger c_1+a c_1^\dagger c_1).$$

Note that this Hamiltonian is not equivalent to the well-known Jaynes-Cummings Hamiltonian of quantum optics. From here on we follow two different approaches. First we discuss analytical solutions within the short excitation pulse limit which are nonperturbative with respect to the electron-phonon coupling. Second, we compare these results with numerical solutions following the usual hierarchy approach. This offers the possibility (i) to translate the results of the simple model to the usual language of the more complex many-body problem in terms of particle correlation functions

and (ii) to test the validity of truncation schemes. We will finally discuss the additional influence of exciton-continuum scattering.

In order to derive closed-form analytical results we describe the dynamics of the system in terms of generating functions for phonon assisted density matrices. This method has recently been formulated also for more general situations in Ref. 41. In our case it is sufficient to follow the time evolution of three dynamical variables defined as

$$Y(\alpha,\beta,t)\equiv\langle c_0^\dagger c_1 \exp(\alpha a^\dagger)\exp(\beta a)\rangle,$$

$$C(\alpha,\beta,t)\equiv\langle c_1^\dagger c_1 \exp(\alpha a^\dagger)\exp(\beta a)\rangle,$$

$$F(\alpha,\beta,t)\equiv\langle \exp(\alpha a^\dagger)\exp(\beta a)\rangle,$$

where α and β are arbitrary complex parameters. All phonon assisted density matrices conventionally used to model the system can be obtained from these functions as derivatives with respect to the parameters α and β taken at $\alpha=\beta=0$. The generating functions Y and C can be regarded as phonon wave packets that correspond to the optical transition amplitude and the occupation density of the upper level, both variables known from the optical Bloch equations. Note that the occupation density of the lower level is redundant due to charge conservation. F is a new dynamical object which is needed to describe correlations in the phonon system including effects of coherent phonons or nonequilibrium (hot) phonon distributions. The most remarkable property of these functions is that straightforward setting up of the Heisenberg equations of motion for these quantities does not lead to a phononic hierarchy problem, instead the following closed set of partial differential equations is obtained:

$$i\partial_t Y=[\Omega+\omega_{\mathrm{LO}}(\beta\partial_\beta-\alpha\partial_\alpha)+g(\beta+\partial_\alpha+\partial_\beta)]Y - \frac{idE}{\hbar}(F-2C),$$

$$i\partial_t C=[\omega_{\mathrm{LO}}(\beta\partial_\beta-\alpha\partial_\alpha)+g(\beta-\alpha)]C-\frac{dE}{\hbar}(Y^T-Y),$$

$$i\partial_t F=\omega_{\mathrm{LO}}(\beta\partial_\beta-\alpha\partial_\alpha)F+g(\beta-\alpha)C,$$

with $Y^T(\alpha,\beta)\equiv Y^*(\beta^*,\alpha^*)$. The partial derivatives can be eliminated by means of the transformations

$$\tilde{Y}(\alpha,\beta,t)\equiv e^{i\bar{\Omega}t+\beta\tilde{g}e^{i\omega_{\mathrm{LO}}t}}Y(\alpha e^{-i\omega_{\mathrm{LO}}t}+\tilde{g},\beta e^{i\omega_{\mathrm{LO}}t}-\tilde{g},t),$$

$$\tilde{C}(\alpha,\beta,t)\equiv e^{\tilde{g}(\beta e^{i\omega_{\mathrm{LO}}t}+\alpha e^{-i\omega_{\mathrm{LO}}t})}C(\alpha e^{-i\omega_{\mathrm{LO}}t},\beta e^{i\omega_{\mathrm{LO}}t}t),$$

$$\tilde{F}(\alpha,\beta,t)\equiv F(\alpha e^{-i\omega_{\mathrm{LO}}t},\beta e^{i\omega_{\mathrm{LO}}t},t),$$

$$\tilde{E}(t)\equiv\frac{d}{\hbar}e^{i\tilde{\Omega}t}E(t),$$

where $\tilde{\Omega}\equiv\Omega-\omega_{\mathrm{LO}}\tilde{g}^2$ and $\tilde{g}\equiv g/\omega_{\mathrm{LO}}$. The result is a set of three ordinary differential equations which can be further simplified by defining functions with only a single complex argument α according to $\tilde{f}(\alpha,t)\equiv\tilde{f}(-\alpha^*,\alpha,t)$ where $\tilde{f}$ stands for $\tilde{Y}$, $\tilde{C}$ or, $\tilde{F}$, respectively. These equations read

$$\partial_t\tilde{Y}(\alpha)=i\tilde{E}\{e^{\alpha\tilde{g}e^{i\omega_{\mathrm{LO}}t}}\tilde{F}(\alpha-\tilde{g}e^{-i\omega_{\mathrm{LO}}t})-2e^{\alpha^*\tilde{g}e^{-i\omega_{\mathrm{LO}}t}} \times\tilde{C}(\alpha-\tilde{g}e^{-i\omega_{\mathrm{LO}}t})\},$$

$$\partial_t\tilde{C}(\alpha)=ie^{-\tilde{g}^2}\{\tilde{E}e^{\alpha\tilde{g}e^{i\omega_{\mathrm{LO}}t}}\tilde{Y}^*(-\alpha+\tilde{g}e^{-i\omega_{\mathrm{LO}}t}) -\tilde{E}^*e^{-\alpha^*\tilde{g}e^{-i\omega_{\mathrm{LO}}t}}\tilde{Y}(\alpha+\tilde{g}e^{-i\omega_{\mathrm{LO}}t})\},$$

$$\partial_t\tilde{F}(\alpha)=-i\tilde{g}\omega_{\mathrm{LO}}2\,\mathrm{Re}[\alpha e^{i\omega_{\mathrm{LO}}t}]e^{-\tilde{g}2\ i\mathrm{Im}[\alpha e^{i\omega_{\mathrm{LO}}t}]}\tilde{C}(\alpha).$$

In order to have a well defined starting point for the dynamics, we will assume the system initially to occupy the lower level and the phonon system to be in thermal equilibrium, leading to the following intial conditions:[41] $\tilde{Y}_0(\alpha)=\tilde{C}_0(\alpha)=0$ and $\tilde{F}_0(\alpha)=\exp(-N_{\mathrm{LO}}|\alpha|^2)$, where $N_{\mathrm{LO}}\equiv 1/[\exp(\hbar\omega_{\mathrm{LO}}/k_BT)-1]$ is the equilibrium (Bose) value of the phonon occupation. Here is the only place where the temperature enters the dynamics. In terms of our final dynamical variables the polarization P and the occupation density of the upper level C_u are given by

$$P(t)=dY(\alpha=0,\beta=0,t)=de^{-(i\tilde{\Omega}t+\tilde{g}^2)}\tilde{Y}(\tilde{g}e^{-i\omega_{\mathrm{LO}}t},t),$$

$$C_u(t)=C(\alpha=0,\beta=0,t)=\tilde{C}(\alpha=0,t).$$

The equations of motion derived above represent the complete dynamics of our model system and allow a numerical treatment for arbitrary coupling strengths of electrons to both phonons and photons. Furthermore, for excitation with a sequence of δ pulses it is easy to obtain analytical results that are nonperturbative with respect to the electron phonon coupling by solving these equations iteratively in the laser field. The simplest case is the linear response to a δ pulse, i.e., $E(t)=E_0\delta(t)$, resulting in a linear polarization

$$P^{(1)}=\frac{id^2E_0}{\hbar}\Theta(t)e^{-i\tilde{\Omega}t+\tilde{g}^2(e^{-i\omega_{\mathrm{LO}}t}-1-N_{\mathrm{LO}}|e^{-i\omega_{\mathrm{LO}}t}-1|^2)}.$$

At zero temperature, where $N_{\mathrm{LO}}=0$, this result can also be written as

$$P^{(1)}=\frac{id^2E_0}{\hbar}e^{-\tilde{g}^2}\Theta(t)\sum_{n=0}^{\infty}\frac{\tilde{g}^{2n}}{n!}e^{-i(\tilde{\Omega}+n\omega_{\mathrm{LO}})t}$$

which shows explicitly the well-known result of phonon sidebands at multiples of the phonon frequency above the polaron shifted energy. It is interesting to note that for a calculation using the conventional approach of truncating the hierarchy at the level of density matrices with single phonon assistence it has been found[17] that the first sideband is $(1+2\tilde{g}^2)\hbar\omega_{\mathrm{LO}}$ above the zero phonon line. Two things can be learned from this analysis: first, for strong electron-phonon coupling the difference to the exact energy spacing $\hbar\omega_{\mathrm{LO}}$ can be quite large resulting in significant deviations between the analytical solution and the result of the first order truncation scheme, even in cases where higher-order sidebands are not excited; second, within our simple model it is not possible to explain any deviation of the frequency of phonon oscillations from the value ω_{LO}. Such shifts have been observed in GaAs samples[6] but are absent in our present experiments on ZnSe, highlighting again the differences between these material systems.

To analyze the effect of strong electron-phonon coupling on the nonlinear optical signal we consider the coherent control setup of Fig. 1(a) as an example. Assuming an excitation with δ pulses, the relevant third-order polarization is given by

$$
\begin{aligned}
P^{(3)}_{2q_2-q_1} = & \frac{-id^4E_0|E_0|^2\Theta(t)}{\hbar^3} e^{-i\tilde{\Omega}t+2\tilde{g}^2[\cos(\omega_{\mathrm{LO}}t)-1]} \\
& \times\{\Theta(-t_1)e^{-\gamma(t-t_1)} \\
& \times e^{-i\tilde{\Omega}t_1+\tilde{g}^2(2e^{-i\omega_{\mathrm{LO}}t_1}-e^{i\omega_{\mathrm{LO}}(t-t_1)}-1)} \\
& \times e^{-\tilde{g}^2N_{\mathrm{LO}}|2-e^{-i\omega_{\mathrm{LO}}t_1}-e^{-i\omega_{\mathrm{LO}}t}|^2} \\
& + \Theta(-t_{1'})e^{-\gamma(t-t_{1'})} \\
& \times e^{-i\tilde{\Omega}t_{1'}+\tilde{g}^2(2e^{-i\omega_{\mathrm{LO}}t_{1'}}-e^{i\omega_{\mathrm{LO}}(t-t_{1'})}-1)} \\
& \times e^{-\tilde{g}^2N_{\mathrm{LO}}|2-e^{-i\omega_{\mathrm{LO}}t_{1'}}-e^{-i\omega_{\mathrm{LO}}t}|^2}\},
\end{aligned}
$$

where, without loss of generality, we have chosen $t_2=0$. In order to make contact with our experiments the square of this polarization has to be integrated with respect to the real time t. As the model by itself does not provide for a decay of the polarization we have accounted in our numerical studies phenomenologically for dephasing by introducing a finite imaginary part for the transition frequency $\tilde{\Omega}$ in the Hamiltonian according to $\Omega\rightarrow\Omega-i\gamma$. To get some feeling for the behavior of the signal we expand the exponentials to first order for the special case $t=0$, $N_{\mathrm{LO}}=0$, $t_{21}>0$, $t_{21'}>0$ and obtain

$$
|P^{(3)}_{2q_2-q_1}|^2 = \mathrm{const}\{1+\cos(\tilde{\Omega}t_{11'})+\tilde{g}^2h(t_{21'},t_{11'})\}
$$

with

$$
\begin{aligned}
h \equiv & \cos\omega_{\mathrm{LO}}t_{21'}\{\cos\omega_{\mathrm{LO}}t_{11'}+1+\cos(\tilde{\Omega}+\omega_{\mathrm{LO}})t_{11'} \\
& +\cos\tilde{\Omega}t_{11'}\}+\sin\omega_{\mathrm{LO}}t_{21'}\{\sin\omega_{\mathrm{LO}}t_{11'}+\sin(\tilde{\Omega}+\omega_{\mathrm{LO}})t_{11'} \\
& -\sin\tilde{\Omega}t_{11'}\}.
\end{aligned}
$$

Due to the expansion, only the zero phonon line and the first sideband contribute. As a function of $t_{21'}$ the signal oscillates as expected with the phonon frequency ω_{LO}. The amplitude of these beats can be controlled adjusting the delay $t_{11'}$; in particular we find a vanishing beat amplitude h for $(\tilde{\Omega}+\omega_{\mathrm{LO}})t_{11'}=(2n+1)\pi$ or $\tilde{\Omega}t_{11'}=(2n+1)\pi$. At these delays either the polarization component with the frequency of the zero phonon line or the first sideband vanishes due to destructive interference. The interference becomes incomplete when a finite damping is taken into account. With damping the behavior in the vicinity of delays $(\tilde{\Omega}+\omega_{\mathrm{LO}})t_{11'}=(2n+1)\pi$ is qualitatively different from $\tilde{\Omega}t_{11'}=(2n+1)\pi$. In the first case the weak contribution from the first sideband is further reduced leading to an almost vanishing beat amplitude. In the second case the amplitude of the strong zero phonon contribution is reduced and now becomes comparable with the contribution of the sideband resulting in a good visibility of the beats at low overall signal amplitudes. This is exactly the behavior found in experiments in the low-coupling limit.[17] In the strong-coupling limit the above expansion is no longer valid and contributions from higher sidebands become noticable. Except for delays where either the zero phonon contribution or the first sideband vanish, contributions from these two lines dominate the signal due to their high oscillator strengths resulting in beats with the phonon frequency. Beats with twice the phonon frequency can become dominant only when the first sideband vanishes. The visibility for these beats depends on how good the condition of similar strengths for the signal components from the zero phonon line and the second sideband can be fullfilled in the corresponding delay range. Similar to the situation in the low-coupling limit this condition crucially depends on the dephasing time.

It is most interesting to compare the analytical results for δ pulses with calculations based on the conventional hierarchy approach. Here, the dynamics is formulated in terms of the phonon assisted density matrices $\rho^{ij}_{kn}\equiv\langle c_i^\dagger c_j(a^\dagger)^k a^n\rangle$. From the Heisenberg equations of motion for these quantities we obtain the following coupled and open set of equations:

$$
\begin{aligned}
\partial_t\rho^{01}_{kn} = & -i[\Omega+(n-k)\omega_{\mathrm{LO}}]\rho^{01}_{kn}+\frac{idE}{\hbar}(\rho^{00}_{kn}-\rho^{11}_{kn}) \\
& -ig(n\rho^{01}_{k,n-1}+\rho^{01}_{k,n+1}+\rho^{01}_{k+1,n}),
\end{aligned}
$$

$$
\begin{aligned}
\partial_t\rho^{11}_{kn} = & i(k-n)\omega_{\mathrm{LO}}\rho^{11}_{kn}+\frac{idE}{\hbar}(\rho^{10}_{kn}-\rho^{01}_{kn}) \\
& +ig(k\rho^{11}_{k-1,n}-n\rho^{11}_{k,n-1}).
\end{aligned}
$$

Similar equations are found for ρ^{10}_{kn} and ρ^{00}_{kn}. We have solved these equations numerically with initial values $\rho^{ij}_{kn}=0$ for all elements, except for $\rho^{00}_{00}=1$, which is appropriate in the limit of zero temperature. The open set of equations is truncated for $k\leqslant k_{\max}$ and $n\leqslant n_{\max}$. In our simulation we have used $k_{\max}=n_{\max}=5$ and solved the truncated set of equations within the rotating wave approximation. The diffracted signal in direction $2\mathbf{q}_2-\mathbf{q}_1$ is extracted by the projection procedure described in Ref. 6.

A comparison between the analytical results for δ pulses and the numerical solutions for finite pulses following the hierarchy approach is shown in Figs. 10 and 11. The parameters correspond to the ZnSe experiment: $\hbar\omega_{\mathrm{LO}}=31.8\,\mathrm{meV}$, $\tilde{g}=0.8$ (GaAs would be $\tilde{g}=0.2$ [(Ref. 17)], $\hbar\tilde{\Omega}=\hbar\omega=2822\,\mathrm{meV}$, $\gamma=1/300\,\mathrm{fs}^{-1}$. For the numerical solutions we have furthermore: $k_{\max}=n_{\max}=5$, and 13-fs sech^2 pulses within the weak excitation density limit, i.e., the pulse area is $\Theta=10^{-4}\pi$. The two approaches used to analyze the simple model of electron-phonon coupling obviously agree very well; compare Figs. 10(a) and (b) and Figs. 11 (a) and (b). In particular, around $t_{11'}=-20\,\mathrm{fs}$, the two-phonon oscillation becomes prominent only in a small regime of values for $t_{11'}$ (Fig. 10). The corresponding interval in $t_{11'}$ is wider around $t_{11'}=-69\,\mathrm{fs}$ (Fig. 11). Also, both of them agree well with the corresponding experimental result (compare Figs. 10 and 11 with Figs. 5 and 6).

Intuitively, the observed behavior can be understood as follows. The relative strengths of the n phonon sideband scales as $\sim\tilde{g}^{2n}/n!$. For $\tilde{g}=0.8$ we have: 1 for $n=0$, 0.8 for $n=1$, 0.2 for $n=2$, 0.04 for $n=3$ and so forth. Obviously, under these conditions only the $n=0,1,2$ contributions are

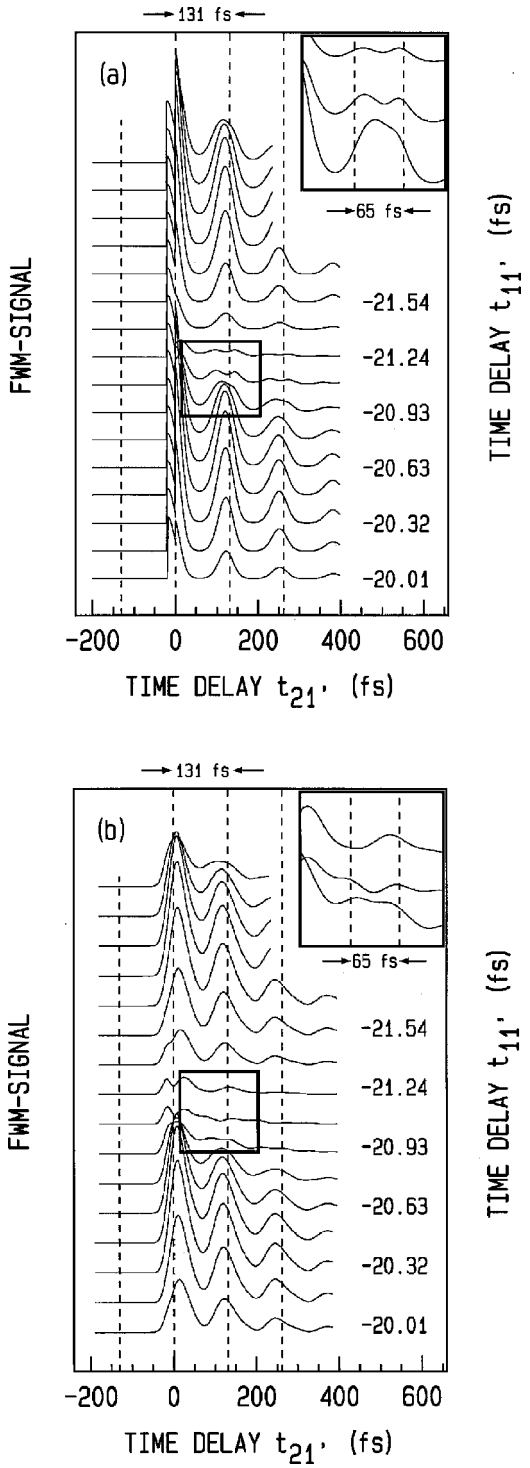

FIG. 10. Model: coherent control under conditions as the experiment (Fig. 5). The inset highlights the prominent two-phonon oscillation. (a) analytical result for δ pulses, (b) numerical solution following the hierarchy approach.

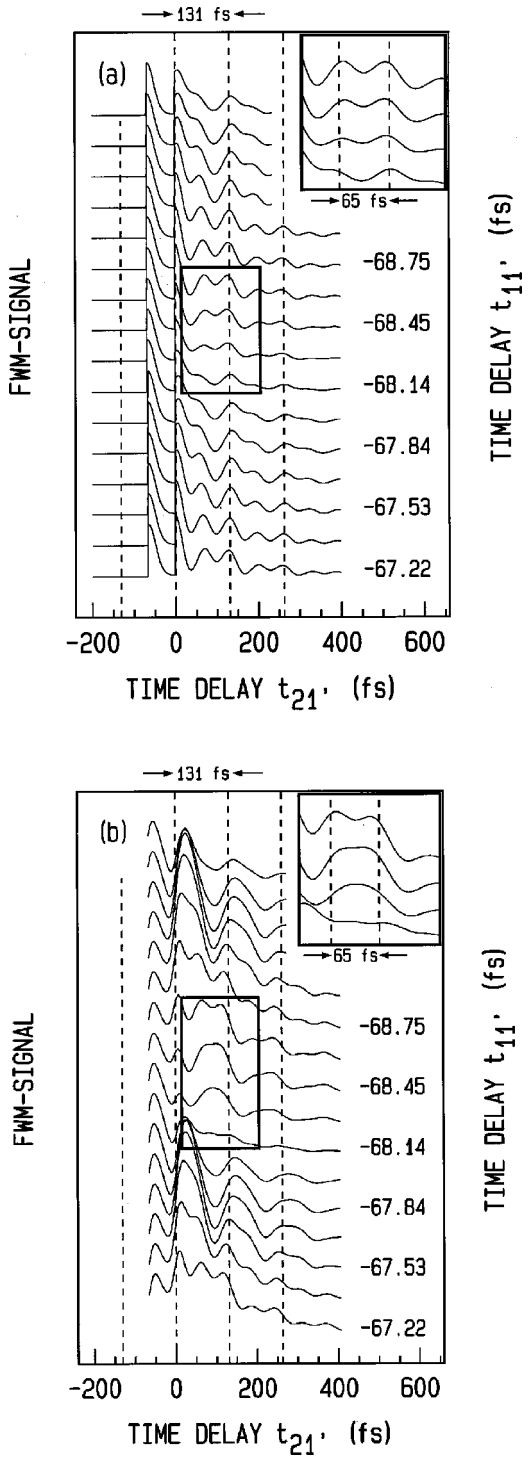

FIG. 11. Model: coherent control under conditions as the experiment (Fig. 6). The inset highlights the prominent two-phonon oscillation. (a) analytical result for δ pulses, (b) numerical solution following the hierarchy approach.

actually important. Destructive interference with respect to the n-phonon contribution means that

$$(\tilde{\Omega}+n\omega_{\mathrm{LO}})t_{11'}=(2m+1)\pi \tag{1}$$

with integer m. This relation is illustrated in Fig. 12 for the parameters used above and corresponding to the intervalls in $t_{11'}$ shown in Figs. 10 and 11. The dots in Fig. 12 are the points of destructive interference. For small time delays $t_{11'}$, the zero-phonon transition, the one-phonon sideband and the two-phonon sideband exhibit a small phase shift [Fig. 12(a)]. Consequently, we can either adjust for destructive interference with respect to the $n=1$ contribution and obtain the prominent two-phonon oscillation (due to a quantum beating between the $n=0$ and the $n=2$ polarizations) or we can adjust for destructive interference for the $n=2$ contribution

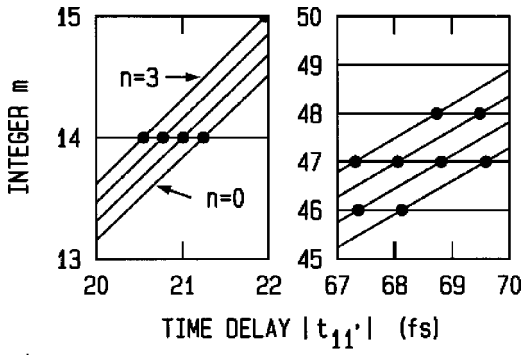

FIG. 12. Illustration of the points of destructive interference (dots) for the n-phonon sidebands: $(\tilde{\Omega}+n\omega_{\mathrm{LO}})\ t_{11'}=(2m+1)\pi$ with integer m. For clarity, only $n=0,1,2,3$ are shown. Parameters correspond to Figs. 10 and 11.

and obtain the prominent one-phonon oscillation. For destructive interference with respect to the $n=0$ contribution, we have very little overall signal. On the other hand, for $t_{11'}$ approximately equal to half the phonon period [Fig. 12(b)], the $n=0$ and the $n=2$ contributions are approximately in phase. Thus $t_{11'}$ effectively modulates the relative weight of the $n=1$ contribution only. Consequently, the two-phonon oscillation is present whenever the FWM signal is of appreciable strength (Fig. 11). Finally, for $t_{11'}$ approximately equal to one phonon period, the $n=0$, $n=1$, and the $n=2$ contributions are always in phase. Thus the *shape* of the FWM signal is almost independent of $t_{11'}$.

While the model accounts for the qualitative behavior of the coherent control experiment rather well, it has a number of shortcomings also: (i) The real time behavior of the FWM signal also exhibits phonon oscillations. This can directly be seen from the analytical expression for $P^{(3)}$. Consequently, the FWM spectra show phonon satellites which are well visible on a linear scale. This is in contradiction with the experimental observation (Fig. 4) and with the complete quantum kinetics theory for the weak electron-phonon coupling regime.[6] (ii) For the simple two-pulse FWM experiment, the model does not show direct indications of two-phonon oscillations—in contrast to the experiment (Fig. 2). (iii) The model does not reproduce the rapid initial decay seen in the experiment (e.g., Figs. 2 and 3). Discrepancy (iii) is very likely due to electron-electron scattering, because the three-pulse experiment on ZnSe (Fig. 8) is very closely similar to the same experiment on GaAs (Fig. 2 in Ref. 39). This unusual line shape has been interpreted in terms of exciton-continuum scattering.[39] If this contribution was added to the simple phonon model discussed here, the agreement with experiment would likely become better.

The three aspects, (i)–(iii), have to be reproduced by a microscopic quantum kinetic theory of electron-phonon scattering in the strong-coupling regime. Such a theory has to include the band continua and one- and two-phonon or even higher-order scattering contributions. Bands of states—unlike our simple model—would also lead to true dephasing due to the electron-phonon coupling. The experimental data strongly suggest that the real time response of the FWM signal is dominated by the $1s$-exciton dynamics. Due to charge neutrality, the $1s$-exciton-phonon coupling is much weaker than the coupling of an unbound electron-hole pair to the phonons. This explains why no phonon satellites are observed in the FWM spectra. The data also suggest that the dynamics in the delay time domain is given by that of the continuum states.

Finally, we relate our work to the recently published theoretical work of Ref. 42. They give reference to our experimental observations, which were available to them by a preprint of this work. Their exact analytical nonperturbative solution of the simple model Hamiltonian for δ-shaped excitation pulses is mathematically identical to the one presented here. Yet, the conclusions derived by the authors in that article[42] are different from ours. Specifically, they state that, in the coherent control geometry, doublets of peaks occur which are separated by the time delay $t_{11'}$ (τ_1 in their nomenclature). While this statement is indeed true in the limit $\tilde{g}\to\infty$, it can easily be falsified for finite values of $\tilde{g}$ by example. A first example has already been given in this article: The inset of Fig. 10(a) shows two peaks which are roughly separated by $\approx$ 50 fs while we have $t_{11'}\approx 21$ fs. Second example: For somewhat larger electron-phonon couplings $\tilde{g}$ than the ones discussed here, it is simple to find several values of $t_{11'}$ where one finds three peaks (rather than just two) within one phonon oscillation period. This contradicts their interpretation in terms of doublets while such behavior can easily by understood within our Fig. 12 and is simply related to a prominent $n=3$ phonon sideband.

V. CONCLUSIONS

The electron longitudinal optical phonon coupling constant increases by about a factor of 10 going from GaAs to the much more polar II-VI semiconductor ZnSe. While one-phonon scattering processes are sufficient to understand the non-Markovian dynamics in GaAs, multiple phonon processes have to be accounted for in ZnSe. Even if a crystal electron emits n phonons in a single step, its coherence is preserved for some time. Thus the initial and final states can still interfere and we observe a quantum beating with n times the LO-phonon frequency. This observation is evidence for quantum kinetics. Certain aspects of the experimental observations can be understood within a simple model which demonstrates the connection to molecular systems: A two-level system coupled to a single phonon mode. This model is solved both analytically and by the infinite hierarchy of density matrices. When treated to sufficient order in the coupling constant, both approaches deliver similar results. Other aspects of the experimental data remain to be explained by a more complete microscopic quantum kinetics theory of non-Markovian electron-phonon scattering in semiconductors.

ACKNOWLEDGMENTS

This work has been supported by the Krupp-Stiftung and the DFG-Schwerpunktprogramm *Quantenkohärenz in Halbleitern*.

[1] H. Haug and A.-P. Jauho, *Quantum Kinetics in Transport and Optics of Semiconductors*, Springer Series in Solid-State Sciences Vol. 123 (Springer-Verlag, Berlin, 1996).
[2] A. V. Kuznetsov, Phys. Rev. B **44**, 8721 (1991).
[3] R. Zimmermann, J. Lumin. **53**, 187 (1992).
[4] M. Hartmann and W. Schäfer, Phys. Status Solidi B **173**, 165 (1992).
[5] H. Haug, Phys. Status Solidi B **173**, 139 (1992).
[6] L. Bányai, D. B. Tran Thoai, E. Reitsamer, H. Haug, D. Steinbach, M. U. Wehner, M. Wegener, T. Marschner, and W. Stolz, Phys. Rev. Lett. **75**, 2188 (1995).
[7] C. Fürst, A. Leitensdorfer, A. Lambereau, and R. Zimmermann, Phys. Rev. Lett. **78**, 3733 (1997).
[8] M. U. Wehner, D. S. Chemla, and M. Wegener, Phys. Rev. B **58**, 3590 (1998).
[9] G. C. Cho, W. Kütt, and H. Kurz, Phys. Rev. Lett. **65**, 764 (1990).
[10] A. P. Heberle, J. J. Baumberg, and K. Köhler, Phys. Rev. Lett. **75**, 2598 (1996).
[11] W. S. Warren, H. Rabitz, and M. Dahleh, Science **259**, 1581 (1993).
[12] M. S. Pshenichnikov, W. P. de Boeij, and D. A. Wiersma, Phys. Rev. Lett. **76**, 4701 (1996).
[13] A. Haché, Y. Kostoulas, R. Atanasov, J. L. P. Hughes, J. E. Sipe, and H. M. van Driel, Phys. Rev. Lett. **78**, 306 (1997).
[14] M. Gurioli, F. Bogani, S. Ceccherini, and M. Colocci, Phys. Rev. Lett. **78**, 3205 (1997).
[15] S. Ogawa, H. Nagano, H. Petek, and A. P. Heberle, Phys. Rev. Lett. **78**, 1339 (1997).
[16] V. Blanchet, C. Nicole, M.-A. Bouchene, and B. Girard, Phys. Rev. Lett. **78**, 2716 (1997).
[17] M. U. Wehner, M. H. Ulm, D. S. Chemla, and M. Wegener, Phys. Rev. Lett. **80**, 1992 (1998).
[18] T. Saiki, K. Takeuchi, K. Ema, M. Kuwata-Gonokami, K. Ohkawa, and T. Mitsuyu, J. Cryst. Growth **138**, 805 (1994).
[19] H. P. Wagner, J. Lehmann, and B. Hahn, J. Lumin. **66**, 84 (1996).
[20] A. J. Fischer, D. S. Kim, J. Hays, W. Shan, J. J. Song, D. B. Eason, J. Ren, J. F. Schetzina, H. Luo, J. K. Furdyna, Z. Q. Zhu, T. Yao, J. F. Klem, and W. Schäfer, Phys. Rev. Lett. **73**, 2368 (1994).
[21] H. P. Wagner, A. Schätz, R. Maier, W. Langbein, and J. M. Hvam, Phys. Rev. B **56**, 12 581 (1997).
[22] H. P. Wagner, A. Schätz, R. Maier, W. Langbein, and J. M. Hvam, Phys. Rev. B **57**, 1791 (1998).
[23] T. Saiki, M. Kuwata-Gonokami, K. Ohkawa, and T. Mitsuyu, Solid State Commun. **95**, 679 (1995).
[24] U. Neukirch, D. Weckendrup, K. Wundtke, J. Gutowski, and D. Hommel, J. Opt. Soc. Am. B **13**, 1256 (1996).
[25] M. Umlauff, J. Hoffmann, H. Kalt, W. Langbein, J. M. Hvam, M. Scholl, J. Söllner, M. Heuken, B. Jobst, and D. Hommel, Phys. Rev. B **57**, 1390 (1998).
[26] R. W. Schoenlein, J.-Y. Bigot, M. T. Portella, and C. V. Shank, Appl. Phys. Lett. **58**, 801 (1991).
[27] S. Backus, M. T. Asaki, C. Shi, H. C. Kapteyn, and M. M. Murnane, Opt. Lett. **19**, 399 (1994).
[28] S. H. Ashworth, M. Joschko, M. Woerner, E. Riedle, and T. Elsässer, Opt. Lett. **20**, 2120 (1995).
[29] D. Steinbach, W. Hügel, and M. Wegener, J. Opt. Soc. Am. B **15**, 1231 (1998).
[30] M. T. Asaki, C. Huang, D. Garvey, J. Zhou, H. C. Kapteyn, and M. M. Murnane, Opt. Lett. **18**, 977 (1993).
[31] R. Szipöcs, K. Ferencz, C. Spielmann, and F. Krausz, Opt. Lett. **19**, 201 (1994).
[32] F. Haché, T. J. Driscoll, M. Cavallari, and G. M. Gale, Appl. Opt. **35**, 3220 (1996).
[33] M. U. Wehner, M. H. Ulm, and M. Wegener, Opt. Lett. **22**, 1455 (1997).
[34] T. Rappen, G. Mohs, and M. Wegener, Phys. Rev. B **47**, 9658 (1993).
[35] J. Petruzello, B. L. Greenberg, D. A. Cammack, and R. Balby, J. Appl. Phys. **63**, 2299 (1988).
[36] H. Wang, K. B. Ferrio, D. G. Steel, Y. Z. Hu, R. Binder, and S. W. Koch, Phys. Rev. Lett. **71**, 1261 (1993).
[37] M. Joschko, M. Woerner, T. Elsässer, E. Binder, T. Kuhn, R. Hey, H. Kostial, and K. Ploog, Phys. Rev. Lett. **78**, 737 (1997).
[38] M. U. Wehner, J. Hetzler, and M. Wegener, Phys. Rev. B **55**, 4031 (1997).
[39] M. U. Wehner, D. Steinbach, and M. Wegener, Phys. Rev. B **54**, R5211 (1996).
[40] M. Wegener, D. S. Chemla, S. Schmitt-Rink, and W. Schäfer, Phys. Rev. A **42**, 5675 (1990).
[41] V. M. Axt and S. Mukamel, Rev. Mod. Phys. **70**, 145 (1998).
[42] H. Castella, and R. Zimmermann, Phys. Rev. B **59**, 7801 (1999).